Journal of Controlled Release 284 (2018) 73–83

Contents lists available at ScienceDirect

Journal of Controlled Release

journal homepage: www.elsevier.com/locate/jconrel

Post-PEGylated and crosslinked polymeric ssRNA nanocomplexes as adjuvants targeting lymph nodes with increased cytolytic T cell inducing properties

Bo Lou[a,1], Ans De Beuckelaer[b,1], George R. Dakwar[c], Katrien Remaut[c], Johan Grooten[b], Kevin Braeckmans[b], Bruno G. De Geest[d], Enrico Mastrobattista[a], Stefaan De Koker[b], Wim E. Hennink[a,*]

[a] Department of Pharmaceutics, Utrecht Institute for Pharmaceutical Sciences, Utrecht University, 3584, CG, Utrecht, The Netherlands
[b] Laboratory of Molecular Immunology, Department of Biomedical Molecular Biology, Ghent University, 9052 Zwijnaarde, Belgium
[c] Laboratory for General Biochemistry and Physical Pharmacy, Ghent University, 9000 Ghent, Belgium
[d] Department of Pharmaceutics, Ghent University, 9000 Ghent, Belgium

ARTICLE INFO

Keywords:
Lymph node
Click chemistry
Adjuvant
ssRNA
Nanocomplexes

ABSTRACT

Potent adjuvants are highly demanded for most protein and peptides based vaccine candidates in clinical development. Recognition of viral single stranded (ss)RNA by innate toll-like receptors 7/8 in dendritic cells results in a cytokine environment supportive to the establishment of long lasting antibody responses and Th1 oriented T cell immunity. To fully exploit the immunestimulatory properties of ssRNA, it needs to be adequately formulated to ensure its optimal delivery to dendritic cells in the vaccine draining lymph nodes. In the present paper, we report on the design of ssRNA nanocomplexes formed by complexation of the cationic poly(carbonic acid 2-dimethylamino-ethyl ester 1-methyl-2-(2-methacryloylamino)-ethyl ester) (pHPMA-DMAE) based polymeric carrier and ssRNA. The resulting ssRNA nanocomplexes were subsequently PEGylated through copper-free click chemistry using PEG-bicyclo[6.1.0]nonyne (PEG-BCN) and cross-linked via disulfide bonds to increase their stability. The obtained near-neutral charged PEGylated ssRNA nanocomplexes (~150 nm) combined ssRNA protection with highly efficient delivery of ssRNA to DCs in the vaccine draining lymph nodes after subcutanuously administration. When co-administrated with a model antigen (soluble ovalbumin (OVA)), ssRNA nanocomplexes were far more efficient at inducing CD8 cytolytic T cells when compared to OVA co-adminstarted with naked ssRNA. Furthermore, IgG2c antibody titers, indicative of Th1 skewed T cell responses, were > 10 times increased by complexing ssRNA into the PEGylated nanocomplexes. This study highlights the potential of post-functionalizing ssRNA nanocomplexes by copper-free click chemistry and these findings indcate that this potent ssRNA adjuvant may profoundly improve the efficacy of a variety of vaccines requiring Th1-type immunity.

1. Introduction

The design of effective immunotherapies against malignancies and insidious intracellular pathogens necessitates improved vaccine adjuvants with a strong capacity to stimulate CD8 cytolytic T cell responses in addition to humoral responses [1–3]. Activation of Toll-like receptors 7 and 8 (TLR7/8) triggers a profound secretion of interleukin 12 (IL-12) and of type I interferons (IFN), the key cytokines that guide the differentiation of CD8+ T cells into cytolytic effector T cells and of CD4+ T cells into Th1 effector cells. Hence, agonists of TLR7/8 have emerged as highly promising vaccine adjuvants to evoke cellular immune responses [4–6]. Guanidine and uridine rich single stranded RNAs (ssRNA) constitute the natural agonists of TLR7/8 present in the endosomes of dendritic cells (DCs), the most potent antigen presenting cells and initiators of T cell immunity [7, 8]. Successful development of ssRNA as vaccine adjuvants, however, requires several hurdles to be taken. As natural ssRNA cannot efficiently penetrate cell membranes and are highly sensitive to ubiquitous RNases, they need to be formulated into nanosized complexes to prevent premature degradation upon injection and to reach the endosomal compartment of DCs. To this

* Corresponding author.
E-mail address: W.E.Hennink@uu.nl (W.E. Hennink).
[1] These authors contributed equally to this work.

https://doi.org/10.1016/j.jconrel.2018.06.010
Received 14 March 2018; Received in revised form 4 June 2018; Accepted 5 June 2018
Available online 15 June 2018
0168-3659/

end, ssRNA have been complexed to liposomes containing cationic lipids including 1,2-dioleoyl-3-trimethylammonium-propane (DOTAP) [9, 10] or to cationic polymers such as polyethyleneimine (PEI) [8] and protamine [11]. Although such approaches indeed have augmented the adjuvanticity of ssRNA, these ssRNA lipoplexes and polyplexes show limited mobility in vivo after local administration, resulting in limited ssRNA prevalence in DCs in the vaccine draining lymph nodes, the crucial sites of induction of adaptive immunity [7]. The limited mobility is most likely caused by the overall positive charge of these lipo/polyplexes which results in binding to extracellular matrix constituents [12–14].

Multiple studies have demonstrated that PEGylation, shields the surface charge and enhances the colloidal stability of nanoparticles and prevents their aggregation upon topical administration, which strongly aids nanoparticle trafficking to the draining lymph nodes [15–17]. Incorporation of poly(ethylene glycol) (PEG) in polyplexes is commonly achieved through the use of PEGylated block copolymers (e.g. PEG-polylysine [18, 19], PEG-poly(aspartamide) [20, 21], PEG-poly(amido amine)s [22, 23] and PEG-PEI [24, 25]) as condensing agents. A major drawback of this strategy is the crowding effect of the neutral polymer (PEG), which hinders proper nucleic acid complexation in dense particles [26–28]. Post-PEGylation – the PEGylation of preformed nucleic acid polyplexes – has emerged as an appealing alternative, with several studies indicating post-PEGylated polyplexes exhibit prolonged circulation times in mice after IV administration [29, 30].

Here we aimed to design a polymeric nanocomplex system, using post-PEGylation via copper free click chemistry [31–33], to efficiently deliver ssRNA to DCs in the lymph node thus enabling effective immunomodulation. Previous studies have demonstrated that poly(carbonic acid 2-dimethylamino-ethyl ester 1-methyl-2-(2-methacryloylamino)-ethyl ester) (pHPMA-DMAE) based nucleic acid delivery systems combine excellent efficiency with a beneficial safety profile [34–37]. pHPMA-DMAE can be hydrolysed at 37 °C and at pH 7.4 (half-life, 9.6 h) [38], enabling removal of the cationic side-chains, to yield pHPMA, a frequently studied water-soluble polymer for drug delivery purposes [39, 40]. Based on this previous work, we designed and synthesized a new series of random copolymers containing reactive azides, poly(HPMA-DMAE-*co*-PDTEMA-co-AzEMAm) (referred as pHDPA, Fig. 1a and Fig. S1a). ssRNA was complexed into polyplexes by electrostatic interaction with cationic pHDPA. The resulting ssRNA polyplexes were subsequently PEGylated through a copper-free chemistry using PEG-bicyclo[6.1.0]nonyne (PEG-BCN) and crorsslinked via disulfide bonds to increase the stability. Upon subcutaneously injection, the generated PEG-pHDPA ssRNA nanocomplexes were expected to increase the amount of ssRNA present in lymph node DCs, which will maximize the adjuvant effect of the immune-stimulatory ssRNA when co-injected with soluble ovalbumin (OVA) protein antigen, especially at the level of the cytolytic T cell response evoked.

2. Materials and methods

2.1. Materials

All chemicals were purchased in the highest purity and used without further purification. Carbonic acid 2-dimethylamino-ethyl ester 1-methyl-2-(2-methacryloylamino)-ethyl ester (HPMA-DMAE) [38] and N-[2-(2-pyridyldithio)]ethyl methacrylamide (PDTEMA) [35, 41] were synthesized as previously reported. 2-Azidoethylmethyacryl amide (AzEMAm) was synthesized as described previously with slightly modification [42]. Lipofectamine 2000 was obtained from Thermo Fisher Scientific (Etten-Leur, The Netherlands). Single chain RNA,luc-mRNA and Cy5-mRNA_luc were purchased from Tebu-bio (TRiLink biotechnologies); Polyuridylic acid [poly(U)] ssPolyU was purchased from InvivoGen. Agarose multi-purpose was purchased from Roche Molecular Biochemicals (Mannheim, Germany). 6 × DNA Loading Dye was purchased from Fermentas (St. Leon-Roth, Germany). SYBR Safe DNA gel stain, Opti-MEM, DMEM medium and dialyzed fetal bovine serum (FBS) were purchased from Life Technologies (Breda, The Netherlands).

2.2. Synthesis and characterization of p(HPMA-DMAE-co-PDTEMA-co-AzEMAm)

p(HPMA-DMAE-*co*-PDTEMA-co-AzEMAm) (pHDPA) was synthesized by radical polymerization under a nitrogen atmosphere. The polymers were synthesized using a monomer to initiator molar ratio

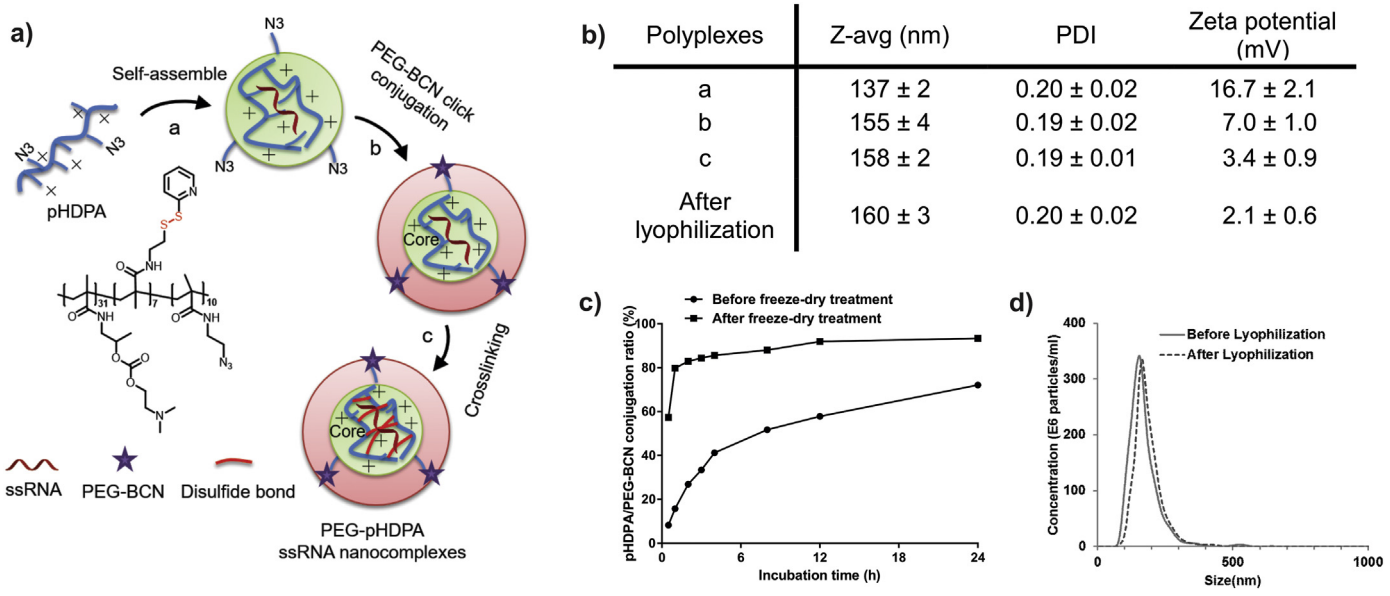

Polyplexes	Z-avg (nm)	PDI	Zeta potential (mV)
a	137 ± 2	0.20 ± 0.02	16.7 ± 2.1
b	155 ± 4	0.19 ± 0.02	7.0 ± 1.0
c	158 ± 2	0.19 ± 0.01	3.4 ± 0.9
After lyophilization	160 ± 3	0.20 ± 0.02	2.1 ± 0.6

Fig. 1. Preparation and characterization of PEG-pHDPA ssRNA nanocomplexes. a) Schematic illustrations of polyplex preparation: (a) self-assembling of the cationic polymer pHDPA and ssRNA; (b) PEG-BCN was clicked on pHDPA polyplexes; (c) crosslinking the polymer chains via the addition of dithiothreitol (DTT). b) Size and zeta-potential of ssRNA polyplexes for each preparation step (n = 3). c) pHDPA and PEG-BCN conjugate efficiency at room temperature at concentration of 64.5 μM for both reactants. d) Size distribution of PEG-pHDPA ssRNA polyplexes before and after lyophilisation/rehydration measured in PBS buffer by Nanosight. The polyplexes were prepared at N/P molar ratio of 4/1 with a final ssRNA concentration of 100 μg/mL.

(M/I) of 50. Different molar feed ratios of HPMA-DMAE, PDTEMA and AzEMAm were used, as shown in Table S1. In a typical experiment to synthesize p(HPMA-DMAE$_{70}$-co-PDTEMA$_{20}$-co-AzEMAm$_{10}$), 200 mg (0.77 mmol) HPMA-DMAE, 56.7 mg (0.22 mmol) PDTEMA, 17 mg (0.11 mmol) AzEMAm and 3.6 mg (0.022 mmmol) AIBN were dissolved in dry DMSO (1 mL) in flasks sealed with rubber septa and subjected to three vacuum-N_2 cycles. The polymerization was carried at 70 °C for 48 h. Next, the polymer was precipated in cold diethyl ether, redissolved in DMF and repeating this procedure 3 times. After extensive dialysis (8 kDa) against an NH_4OAc buffer of pH 5.0 (10 mM, last step 5 mM) at 4 °C, the polymer was collected after freeze drying. The yield of polymer is between 30 and 40%.

The molecular weights and polydisperisity (M_w/M_n) of pHDPA were determined by size exclusion chromatography (SEC) analysis using a Viscotek-GPCmax (Viscotek, Oss, The Netherlands) light scattering (λ = 670 nm, right (90°) and low (7°) angle)/viscosimetric detection system, using ultrahydrogel 2000 7.8 × 300 mm columns in series with a ultrahydrogel 6.0 × 40 mm guard column and 0.3 M NaAc pH 4.4, 30% acetonitrile as eluent [43]. The flow rate was 0.6 mL/min and the run time was 60 min. PolyCALTM PEO standards (Mn = 24 kDa, PDI = 1.01, Malvern) was used for calibration. The copolymer composition was determined by ^{1}H NMR analysis performed with a Gemini 400 MHz spectrometer (Varian Associates Inc., NMR Instruments, Palo Alto, CA) in D_2O. The ratio HPMA-DMAE/PDTEMA/AzEMAm was determined by comparison of the integrals at δ 4.3 ppm (bs, OCH2CH2, HPMA-DMAE), δ7.69 ppm (bs, pyridyl group proton, PDTEMA) and δ3.14–3.51 ppm (m, CH2CH2N3, AzEMAm) (δ4.3/δ7.69/(δ4.08/2).

2.3. Synthesis of PEG-BCN and BCN-PEG-Cy5

NH_2-PEG$_{5000}$-COOH (100 mg, 0.02 mmol, 1 equiv), and cyclooctyne-NHS (BCN-NHS; 9.0 mg, 0.024 mmol, 1.2 equiv) and triethylamine (8.5 μL, 0.06 mmol, 3 equiv) were dissolved in 1.3 mL DMSO, the reaction mixture was stirred at room temperature overnight. The final product was precipitated in cold ether twice, then dissolved in milliQ water, followed by dialysis against water (MWCO: 3000) for 2 days. After filtration and freeze-drying, the polymer was obtained as a white powder. Yield 90 mg, 85.7%. ^{1}H NMR (400 MHz, DMSO): δ = 7.05(s, 1H;OC(=O)NH), 7.05(s, 1H;C=ONH), 4.52 (t, 2H; PEG-OH),4.00 (d, 2H; BCN-CH2-O(=O)), 3.66 (t, 2H; PEG-CH_2), 3.48 (bs, 440H; PEG), 3.04 (s, 2H; OCONHCH_2), 2.90 (s, 2H; C═ONHCH_2), 2.0–2.21(m, 4H; CH_2C(=O)NH_2, alkane),1.99 (m, 2H; NHCH_2CH_2),1.69–1.41 (m, 6H; alkane), 1.54–1.13 (m, 1H; alkane), 0.80–0.71 (m, 2H; alkane) (Fig. S3).

To conjugate Cy5 to PEG-BCN, 50 mg of PEG-BCN (0.0095 mmol) was first dissolved in 1 mL DMSO, 2.34 mg of dicyclohexylcarbodiimide (DCC,0.0114 mmol) and 1.32 mg of N-hydoxysuccinimide (NHS, 0.0114 mmol) were added and stirred for 4 h at room temperature. Then, 7.45 mg of Cy5-amine (0.0114 mmol) and 3.48 mg of triethylamine (0.0342 mmol) were added to the mixture. After overnight reaction, the mixture was diluted with water (10 mL), followed by dialysis against water (MWCO: 3000) for another 2 days. Next, the solution was filtered with 0.2 μm filter and freeze-dried. The resulting polymer was obtained as blue powder. The success of Cy5 coupling was confired by ^{1}H NMR, and no free Cy5 was present in the conjugate as confirmed by SEC analysis.

2.4. Reaction of PEG-BCN with polymer-azide (pHDPA2)

pHDPA2 and PEG-BCN were separately dissolved in 10 mM HEPES buffer (pH 7.4) at a concentration of 10.0 mg/mL (4.9 mM of azide groups) and 20 mg/mL (3.7 mM of BCN groups), respectively. Samples of the polymer solution (13.2 μL) and PEG-BCN solution (17.3 μL, azide/BCN molar ratio 1:1 or 8.7 μL, azide/BCN molar ratio 2:1) were mixed and diluted with 10 mM HEPES buffer (pH 7.3) (69.5 μL or 78.2 μL). The reaction mixtures were incubated at room temperature and collected at incubation times of 0, 1, 2, 3, 4, 8, 12 and 24 h.

The collected samples were analyzed by size exclusion chromatography (SEC) described in the previous section. The unreacted PEG-BCN concentration was calculated based on RI peak intensity using a PEG-BCN calibration curve (Fig. S3d). For the sample with freeze-dry treatment, the reaction mixture (after reacted at RT after defined time as mentioned above) were rapid frozen using liquid nitrogen. The polymer was collected after freeze drying and subsequently dissolved in water (100 μL) and analyzed by SEC. For the sample with freeze-thaw treatment, the reaction mixture (after reacted at RT after defined time as mentioned above) were frozen at −30 °C for 16 h and thawed at 4 °C for 2 h.

2.5. Preparation of RNA polyplexes

For the preparation of RNA polyplexes, 3-steps can be distinguished, namely complexation, post-PEGylation, and crosslinking (Fig. 1a). In a typical example, polyplexes were prepared at N/P molar ratio of 4, with RNA concentration of 100 μg/mL. pHDPA2 and BCN-PEG were first dissolved in 10 mM HEPES buffer, pH 7.4 with a concentration of 10 mg/mL. Next, 28.8 μL of pHDPA2 was diluted with 100 μL HEPES buffer and the resulting solution was added to 260 μL ssRNA (60 μg, HEPES buffer) solution, vortexed fot 5 s and incubated on ice for 10 min. Next, 76.4 μL of BCN-PEG was added to the polyplex mixture and incubated at room temperature for 2 h. Polyplexes were subsequetly crosslinked by addition of 14.5 μL dithiothreitol (DTT, 5 mM dissolved in water) corresponding with a half molar equivalent to PDS groups of pHDPA2, for 1 h at room temperature. After addition of 60 μL sucrose (50% in water) to a final concentration 5% and 15.6 μL NaCl (5 M in water) to a final salt concentration of 150 mM, the polyplexes were frozen in liquid nitrogen and freeze-dried. The obtained cake was resuspended in RNAase-free water (600 μL, final RNA concentration of 100 μg/mL) for further use.

2.6. Determination of the content of free pHDPA2 in RNA polyplexes dispersion

pHDPA2/RNA polyplexs (100 μg/mL) without PEGylation and crosslinking were formulated in 500 μL 10 mM HEPES or PBS buffer at N/P ratios from 2 to 12 as described above. After complexation and incubation at room temperature for 10 min, the polyplex disperion was added to 50 μL NaCl (1.65 M) for 4 h incubation to cause polyplexes aggregation, followed by centrifugation (15,000 rpm for 60 mins) to pellet the aggregated polyplexes [44]. The supernatant was separated and the amount of free polymer was quantified by UV spectroscopy. Briefly, 90 μL of the supernatant was removed and combined with 10 μL of freshly prepared DTT solution (100 mM). After incubating these samples for 30 mins at room temperature, the UV absorbance at 343 nm was measured to determine the amount of free polymer. The concentration of free pHDPA2 in the supernatant was quantified using a calibration curve of varying amount pHDPA2 with the same treatment. The percentage of pHDPA2 polymer associating with ssRNA using following formula: $100–100 * ((W_{total} - W_{free}) / W_{total})$, where W_{total} means total amount of pHDPA2 used to prepare ssRNA polyplexes and W_{free} means amount of free pHDPA2 in polyplexes dispersion.

2.7. Evaluation of post-PEGylation efficiency of PEG-BCN to the polyplexes (ultrafiltration methods)

An ultrafiltration method instead of Vivaspin was used, because it enables a higher recovery efficiency of BCN-PEG-Cy5 and PEGylated pHDPA (~95%), and polyplexes particles (> 80%), by using polyethersulfone ultrafiltration membrane (MWCO, 300 kDa). The RNA polyplexes were post-pegylated with BCN-PEG-Cy5 as mentioned above. The polyplexes dispersion (50 μg/mL) was then purified by ultrafiltration with an Amicon® selector valve with 10 mM HEPES buffer,

pH 7.4, to remove unreacted BCN-PEG-Cy5. After the buffer was exchanged 10 times, the concentrate was analyzed by UV spectroscopy at wavelength 200–700 nm. The RNA and PEG-Cy5-BCN concentration were quantified by measuring the UV absorbance at 260 and 646 nm, respectively.

2.8. PEGylation conjugation efficiency determined by fluorescence correlation spectroscopy (FCS)

The BCN-PEG-Cy5 coupling efficiency after incubation with RNA polyplexes in 10 mM HEPES pH 7.4 for 3 h at room temperature was determined by FCS as previously described by Buyens et al. [23, 36]. Briefly, FCS measurements were performed using free BCN-PEG-Cy5 ($\lambda_{excitation}$ = 646 nm and $\lambda_{emission}$ = 662 nm) and RNA encapsulated in PEG-pHDPA polyplexes (0.5 μg/mL), on a C1si laser scanning confocal microscope (Nikon, Japan), equipped with a time-correlated single photon counting (TCSPC) data acquisition module (Picoquant, Berlin,-Germany), and water immersion objective lens (Plan Apo 60×, NA 1.2, collar rim correction, Nikon, Japan). During the measurements, the glass bottom 96-well plate (Grainer Bio-one, Frickenhausen, Germany) was covered with adhesive plates seals (ThermoScientific, U.K.) to avoid evaporation of water. For each sample, fluorescence intensity fluctuations were recorded using Symphotime (Picoquant, Berlin, Germany), during 1 min in triplicate. Because the baseline fluorescence intensity of the fluorescence fluctuation profiles recorded by FCS is proportional to the concentration of BCN-PEG-Cy5, the percentage of conjugated and free form BCN-PEG-Cy5 can be calculated as described by Buyens et al. [36].

2.9. Particle size and zeta-potential measurements

The size of the polyplexes was measured with DLS using an ALV CGS-3 system (Malvern Instruments, Malvern, UK) equipped with a JDS Uniphase 22 mW He—Ne laser operating at 632.8 nm, an optical fiber-based detector, a digital LV/LSE-5003 correlator with temperature controller set at 25 °C. The zeta-potential (ζ) of the polyplexes was measured using a Malvern Zetasizer Nano-Z (Malvern, UK) with universal ZEN 1002 'dip' cells and DTS (Nano) software (version 4.20) at 25 °C. Polyplex measurements were performed in 10 mM HEPES pH 7.4 and a RNA concentration of 15 μg/mL.

The size distribution of the polyplexes was also detemined by nanoparticles tracking analysis (NTA) using a NanoSight LM 10SH (NanoSight, Amesbury, United Kingdom), equipped with a sample chamber with a 532 nm Laser. Typically, RNA polyplexes were diluted with PBS to a concentration of 0.5 μg/ml and measured for 120 s with manual shutter and gain adjustments. The captured videos were analyzed by the NTA 2.0 image analysis software.

2.10. Stability study using fluorescence single particle tracking (fSPT)

fSPT was performed to measure the stability of the PEG-pHDPA Cy5-RNA nanocomplexes in 10% serum. fSPT is a fluorescence microscopy technique that uses widefield and a fast and sensitive CCD camera to record movies of diffusion particles in fluids. These movies were analyzed using in-house developed software, to obtain size distributions as previously described [45].

2.11. Gel retardation study

Polyplex (in)stability was studied by addition of dithiothreitol (DTT) (as reducing agent) and/or heparin (as counter polyanion) and/or serum. Two microliters of DTT (100 mM) and/or 1 μL heparin sodium salt (50 mg/mL) and/or 2.5 μL FBS were added to 20 μL of polyplex dispersion in HBS (40 μg/mL of RNA) yielding a final concentration of 10 mM DTT, 200 μg/mL heparin, and 10% serum. After 0.5 h incubation at 37 °C, for the sample incubated with 10% serum, 4 μL of 0.5 M EDTA (pH 8.0) was added and the sample was then placed on ice for 10 min. Next, 20 μL of the sample was mixed with 3 μL 6 × Loading Dye and loaded into 1% agarose gel in Tris–acetate–EDTA (TAE) buffer containing GelGreen (Biotium). Electrophoresis was done at 120 V for 30 min. RNA was detected using a Gel Doc™ XR + system (BioRad Laboratories Inc., Hercules, CA) with Image Lab software.

2.12. DC2.4 maturation and cellular uptake

DC2.4 cells were seeded into 96-well plate (10^5 cells/ well) and incubated for 24 h. Cy5-mRNA_luc was loaded to the PEG-pHDPA nanocomplexes (N/P 4) as described above. The cells were treated with nanocomplexes (0.25 μg Cy5-RNA) for 24 h with serum. Next, the cells were incubated with 0.4% trypan blue-containing PBS buffer for 5 min and washed with PBS. Internalized RNA polyplexes were examined by flow cytometry (Canto II, BD). To measure the maturation level of D2.4 cells, after incubation cells with ssPolyU PEG-pHDPA nanocomplexes for 24 h, the cells were washed with FACS buffer and subsequently stained with anti-CD40-FITC and anti-CD86-PE antibodies (2 μg/mL, 50 μL per well, eBioscience) for 30 min on ice. These D2.4 cells were subsequently analyzed by flow cytometry after being washed with FACS buffer.

2.13. Mice

Female wild type C57BL/6 mice were purchased from Janvier (Le Genest Saint Isle, France). OT-I mice carrying a transgenic $CD8^+$ T cell receptor specific for the MHC I-restricted ovalbumin (OVA) peptide SIINFEKL were donated by Dr. Bart Lambrecht from Ghent University (Ghent, Belgium). All mice were 7–12 weeks old at the start of the experiment and maintained under specific pathogen-free conditions. Animals were treated according to the European guidelines for animal experimentation. All experiments were approved by the local ethical committee for animal experiments of Ghent University (Ghent, Belgium).

2.14. Drainage of Cy5-labeled ssRNA polyplexes to popliteal lymph nodes

C57BL/6 mice were subscutanously injected with Cy5-mRNA_luc loadded PEG-pHDPA nanocomplexes and DOTAP ssRNA lipoplexes using DOTAP/DOPE at N/P ratio of 1 (Avanti Polar Lipids, Alabaster, AL, USA), referred as DOTAP ssRNA, in the footpad. The injected dose of RNA was 5 μg (20 μl in 5% glucose HBS buffer). Popliteal lymph nodes were isolated 24 h post injection and analyzed by flow cytometry. Cells were stained with α-CD16/CD32 (BD Biosciences, San Diego, CA, USA) to block non-specific FcR binding, and with Live/Dead Fixable Aqua stain (Invitrogen) to eliminate dead cells. Antibodies used were MHC-II-FITC, α-CD11c PerCP-Cy5.5, α-F4/80 PerCP (all BD Biosciences, San Diego, CA, USA). Analysis was performed on a triple-laser (B-V-R) LSR-II (Becton Dickinson, San Jose, CA, USA) followed by FlowJo (Treestar, OR) data processing.

2.15. $CD8^+$ T cell dextramer staining

Subcutaneous immunizations were performed in C57BL/6 mice twice at tail base in a 3 week interval (Fig. 5a). Ten μg of ssPolyU loadded PEG-pHDPA nanocomplexes or DOTAP/DOPE lipoplexes (as mentioned above), together with 10 μg soluble OVA protein (InvivoGen) in a total volume of 40 μl of 5% glucose in water (Ambion, Life technologies, USA). The formulations were injected at tail base of the mice. Five days after last boost injections, blood samples were taken and red blood cells were removed using ACK lysis buffer (BioWhittaker, Wakersville, MD, USA). Cells were stained with α-CD16/CD32 (BD Biosciences, San Diego, CA, USA), Live/Dead Fixable Aqua stain (Invitrogen), α-CD8 PerCP, α- CD3 pacific blue, α-CD19 APC-Cy7 (all BD Biosciences, San Diego, CA, USA) and MHC dextramer H-2 K_b/

SIINFEKL-PE (Immudex, Copenhagen, Denmark).

2.16. Cytotoxic T lymphocyte activity in vivo

Mice immunized with different formulations were same as described above. Two weeks after last boost injection, mice were injected intravenously with 1.5×10^7 target splenocyte cells. Splenocytes were pulsed with 1 μg/ml of MHC-I OVA peptide (SIINFEKL, Invitrogen) or HIV-1 Gag peptide (AnaSpec) as a control before labelling with 5 μM (Termed $CFSE^{hi}$) or 0.5 μM (termed $CFSE^{low}$) 5-(and 6)-carboxyfluorescein diacetate succinimidyl ester (CFSE, Invitrogen), respectively. Labeled cells were mixed at a 1:1 ratio and were adoptively transferred into immunized mice. Two days later, splenocytes from host mice were analyzed by flow cytometry after staining with α-F4/80 (BD Biosciences, San Diego, CA, USA) to exclude auto-fluorescent macrophages. Percentage antigen-specific killing cells was determined using the following formula: $100–100 * ((\%\ CFSE^{hi}\ cells / \%\ CFSE^{low}\ cells)^{immunized\ mice} / (\%\ CFSE^{hi}\ cells / \%\ CFSE^{low}\ cells)^{non\text{-}immunized\ mice}$.

2.17. Measurement of Ab titers

To measure the OVA specific Ab titers, 96-well plates were coated with 100 μl of a 10 μg/ml OVA solution overnight at 4 °C. The plates were washed (1 × 5 min) with washing buffer (PBS containing 0.05% Tween 20) and incubated for 2 h with blocking buffer (PBS containing 2% BSA and 0.05% Tween 20). After blocking, the plates were incubated with 5-fold serially diluted (blocking buffer) serum starting with a dilution of 1:50 for 2 h. To detect bound antiboies, the plates were washed (3 × 5 min) and incubated for 1 h with HRP-conjugated anti-mouse total IgG1and IgG2c Ab (Southern Biotech, Birmingham, AL) with a dilution of 1:3000 in blocking buffer. After the plates were washed (3 × 5 min), 100 μl TMB substrate solution (Sigma-Aldrich, The Netherlands) was added to each well to initiate the color reaction at room temperature in the dark for 30 min. The reaction was stopped with 2 N H_2SO_4 (50 μL/well), and the OD was measured at a wavelength of 450 nm (OD_{450}).

3. Results and discussion

3.1. Polymer synthesis and characterization

2-Azidoethylmethyacryl amide (AzEMAm) (Scheme S1a, Fig. S2) was used to introduce azide moieties in the copolymer structure to enable post polyplex modification using click chemistry. A series of pHDPA with different number of azide units were synthesized by free radical polymerization in dry DMSO (at a fixed monomer/initiator molar ratio of 50/1) (Fig. 1a and Fig. S1). The characteristics of the synthesized polymers (molecular weights determined by SEC and compositions determined by ^1H NMR (Fig. S1b)) are shown in Table S1. This table shows AzEMAm content of the copolymers is higher than that in the feed (feed: 5 to 20 mol%, copolymer contents: 17 to 27 mol%). The incorporation of pyridine disulfide groups (PDS) in the obtained polymers was determined by NMR analysis and was in agreement with the values obtained by UV spectroscopy, used to calculate the amount of dithiothreitol (DTT) needed to crosslink the polyplexes. Table S1 also shows that the molecular weights of the obtained polymers were around the same (~ 10 kDa). pHDPA2 has highest amount of PDS groups of the three polymers, which are favourable for high cross-link density, and enough moieties of azide (~ 10 units per polymer chain) for post-PEGylation; this polymer was therefore selected for the further studies.

The clickable PEG-BCN was synthesized by coupling (1R,8S,9s)-Bicyclo[6.1.0]non-4-yn-9-ylmethyl N-succinimidyl carbonate (BCN-NHS) to the amine group of the distal end of a PEG chain (M_n ~ 5000 Da) (Scheme S1b), as confirmed by ^1H NMR analysis (Fig. S3). The coupling efficiency between PEG-BCN and azide containing pHDPA (pHDPA2) was studied at room temperature in aqueous solution (10 mM HEPES, pH 7.4). The conjugation was confirmed by FTIR analysis (Fig. S4; disappearance of the N_3 vibration at 2130 cm^{-1}) and quantified by size exclusion chromatographical (SEC) analysis (Fig. S5). The conjugation efficiency of pHDPA and PEG-BCN was time (Fig. 1c) and concentration (Fig. S5b) dependent. These figures show that a higher coupling degree was reached at higher concentration and longer incubation time. At BCN/N_3 molar ratio of 1/1, after 3 h incubation with a reactant concentration of 64.5 μM, the conjugation efficiency was 33%. Interestingly, it was found that freeze-drying of the reaction mixture accelerated the conjugation efficiency (Fig. 1c). After a 1 h reaction at room temperature followed by a freeze-drying treatment, the conjugation ratio was 80%, whereas it was only 17% before freeze-drying. The higher conjugation efficiency is likely caused by the increased micro-environmental reactant concentration as a consequence of the freeze-drying process, which leads to a high chance of coupling. It should be mentioned, the conjugation efficiency was also increased by only freeze-thawing (freeze at −30 °C and thaw at 4 °C) the reactant mixture (Fig. S5c), which is in line with previously published results of the reaction of azide modified siRNA and dibenzocyclooctyne (DBCO) modified PEG [46].

3.2. PEG-pHDPA ssRNA nanocomplexes preparation and characterization

PEG-pHDPA ssRNA nanocomplexes were formed via a three steps process as illustrated in Fig. 1a. We first evaluated the self-assembly behaviour of pHDPA and ssRNA (step a). It was shown that ssRNA was completely bound to the polymer at nitrogen/phosphate (N/P) ratios above 1 (Fig. S6a). ssRNA release upon the addition of negatively charged heparin proved that ssRNA complexation is reversible. To obtain particles with a small size, an N/P ratio of 4 instead of 2 was selected for further studies, resulting polyplexes of around 150 nm with zeta potential of 16 mV (Fig. S6b). In step b, the ssRNA polyplexes were post-modified with PEG-BCN. As shown in Fig. S7a, the zeta potential of the polyplexes decreased as a function of time upon incubation with PEG-BCN due to shielding of the surface charge of the particles by the coupled PEG chains. The zeta potential remained stable after 2 h incubation (~10 mV), indicating the post-PEGylation was completed. Conversely, incubation with non-functionalized PEG had no effect on the zeta potential, which means that the shielding was indeed due to the covalent coupling of PEG chains to the surface of the polyplexes. Different amount of PEG-BCN were added to polyplexes to establish under which conditions the surface charge of polyplexes was efficiently shielded with a minimum unreacted amount of BCN-PEG in solution. Fig. S7b shows that at PEG-BCN/N_3 molar ratios above 0.6, no further reduction of the zeta potential (~10 mV) was observed (3 h incubation). Therefore, a PEG-BCN/N_3 ratio of 0.6 was chosen for further experiments. Previous studies demonstrated that disulfide crosslinked polyplexes have a better colloidal stability than their non-crosslinked counterparts, even in the presence of serum [47, 48]. In step c, DTT was added at half molar equivalent to the pyridine disulfide groups of the polymer to induce self-crosslinking via disulfide bonds formation [49]. This final step yielded PEGylated and crosslinked polyplexes with near neutral surface charge and a diameter of 158 nm (Fig. 1b). Notably, the polyplexes' PDI (~0.2) and intensity of the scattered light (data not shown) remained stable during this step, proving that crosslinking of the polyplexes resulted in neither destabilization nor aggregation of the polyplexes. Importantly, the size of PEG-pHDPA ssRNA nanocomplexes was similar before and after lyophilization (Fig. 1b & d) and this dry powder form could be stored at 4 °C for at least 4 weeks without negatively affecting its size and size distribution after rehydration of the polyplexes in buffer.

To quantify the amount of PEG coupled to the ssRNA polyplexes, we first determined the amount of free cationic polymer pHDAP2 in the polyplex dispersion. It has been well documented that for most polyplex formulations, free polymer chains are present in the dispersion [44,

50–52]. Here we used precipitation method (by incubating ssRNA polyplexes with 150 mM NaCl to cause polyplexes aggregation followed by centrifugation) combined with UV analysis to determine the content of uncomplexed pHDPA chains in the ssRNA polyplex dispersion. As shown in Fig. S8, around 60% of pHDPA associated with ssRNA when the polyplexes were prepared at N/P molar ratio of 4. With correction for amount of free polymer present in the polyplexes dispersion, the conjugation efficiency of the PEG-BCN and the pHDPA/ssRNA polyplexes was determined via ultrafiltration method using Cy5-labled PEG-BCN (Scheme S1b). It is noted that after ultrafiltration, the polyplexes size and PDI were stable (data not shown). By measuring the UV absorbance of Cy5 and ssRNA in the concentrate, the amount of PEG-BCN coupled to the polyplexes surface was calculated and it turned out that around 15 mol% of the azide groups of the polyplexes was successfully modified with PEG-BCN (Fig. S9a). This means that on the average each polymer had been modified with 1.5 units of PEG. To further verify the PEG conjugation efficiency by post-PEGylation, fluorescence correlation spectroscopy (FCS) analysis was applied (Fig. S9b) [53]. After incubation of the polyplexes with BCN-PEG-Cy5, the decrease of the fluorescence signal of Cy5 pointing to the coupling of BCN-PEG-Cy5 to the ssRNA polyplexes. After 3 h incubation, the conjugation efficiency was calculated to be around 17%, which is in good agreement with the results of Fig. S9a (~15%).

3.3. PEG-pHDPA ssRNA nanocomplexes stability

The stability and nuclease resistance of PEG-pHDPA ssRNA nanocomplexes was investigated in the presence of serum using fluorescence single particle tracking (fSPT) analysis and a gel retardation assay (Fig. 2). fSPT is a microscopy technique that allows to visualize the movement of individual fluorescently labeled nanoparticles in a certain medium [54, 55]. As shown in Fig. 2a, the size distribution of polyplexes formulated with Cy5-labeled ssRNA did not show significant changes after 2 h incubation in 10% serum, which demonstrates an excellent colloidal stability of these PEGylated polyplexes. Agarose gel retardation study was conducted to test whether the loaded ssRNA in the polyplexes is protected against degradation by RNases present in serum. Fig. 2b shows that after incubation of the polyplexes with 10% serum, the ssRNA band of PEG-pHDPA nanocomplexes was detected on the top (lane 7). In contrast, naked ssRNA was fully degraded during the same conditions (lane 6). Besides, DTT (10 mM) was added to ssRNA polyplexes to break the disulfide bonds of the crosslinks. Fig. 2b (lane 3) shows that only part of the entrapped ssRNA was released in the presence of DTT. Likely, the non-crosslinked cationic polymers still complexed ssRNA. Indeed, when heparin (as counter polyanion) was added, the pHDPA/ssRNA nanocomplexes dissociated and ssRNA was fully released (lane 4).

3.4. In vitro DCs cellular uptake and maturation

To fulfil its role as an adjuvant, ssRNA needs to reach the endosomal compartment of DCs where it can trigger TLR7/8 [56]. When the crosslinked ssRNA polyplexes without PEG coating were prepared (similar procedure as Fig. 1a without step b), severe aggregation of polyplexes was observed, which may due to the inter-polyplexes crosslinking after DTT addition. Therefore, benchmark DOTAP ssRNA lipoplexes (~250 nm with zeta potential −20 mV) were used as a control. The cellular uptake of non-complexed (free) ssRNA, and PEG-pHPDA ssRNA nanocomplexes by DC2.4 cells was investigated using Cy5 labeled ssRNA. Flow cytometric analysis as well as confocal imaging revealed a strong internalization of ssRNA by DCs in the form of DOTAP and PEG-pHDPA nanocomplexes, while low uptake of ssRNA in its free form was observed (Fig. 3a & b). As shown in Fig. 3b, a higher cellular uptake of DOTAP ssRNA lipoplexes compared to PEG-pHDPA ssRNA nanocomplexes was observed, which may due to the bigger size of the lipoplexes than the polyplexes (250 vs 150 nm; particle size plays an important role in DCs cellular uptake [57]).The confocal images were analyzed for colocalization of Cy5-labeled ssRNA and Lysotracker using ImageJ software (Fig. S10). The obtained results demonstrate that most of PEG-pHDPA nanocomplexes were trapped in organelles such as late endosome/lysosomes as evident from their colocalization with the green organelles, compared with DOTAP ssRNA lipoplexes (Pearson's colocalization coefficient: 0.70 vs 0.15 for PEG-pHDPA ssRNA nanocomplexes and DOTAP ssRNA lipoplexes, respectively). This might be ascribed to the low buffering capacity of pHDPA (pKa~9.5) [58] at pH values of the late endosome/lysosomes. Therefore, PEG-pHDPA ssRNA nanocomplexes will be retained in the endosome after cellular endocytosis. On the other hand, the DOTAP lipoplexes are taken up by DCs via macropinosomes and eventually merge with acidic lysosomal compartment [9, 59]. The endosomal TLRs7/8 are crucial sites of interaction with ssRNA for immune stimulation, and consequently the trapped PEG-pHDPA ssRNA nanocomplexes in the endosomes enhanced the immune-stimulatory activity of ssRNA (Fig. 3c). This figure indeed shows that PEG-pHDPA ssRNA nanocomplexes evoked DCs maturation by upregulating of CD40 and CD86 expression on the surface of DC2.4 cells. Considering that both naked ssRNA and soluble PEG-pHDPA

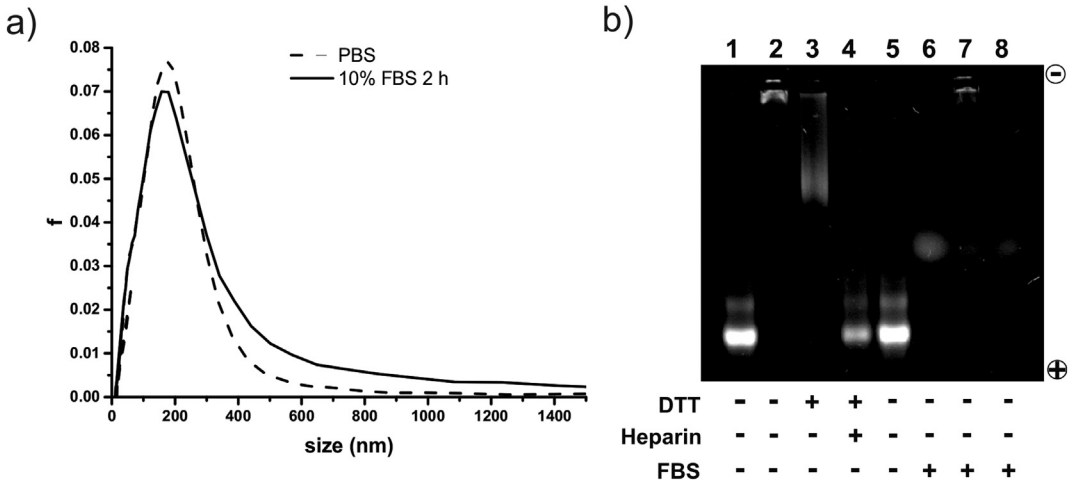

Fig. 2. Stability and nuclease resistance of PEG-pHDPA ssRNA nanocomplexes. a) Size distribution of PEG-pHDPA polyplexes of Cy5-mRNA_luc after incubation with 10% of serum at 37 oC for 2 h measured via fSPT. b) Agarose gel retardation assay of PEG-pHDPA ssRNA nanocomplexes with different treatments. Polyplexes were incubated with 10 mM DTT or 10% FBS for 0.5 h at 37 oC and subsequently incubated with heparin (final concentration of 200 μg/mL) before loading into the agarose gel. Lane 1&5–6: naked ssRNA; Lane 2–4&7: PEG-pHDPA ssRNA polyplexes; Lane 8: 10% FBS only.

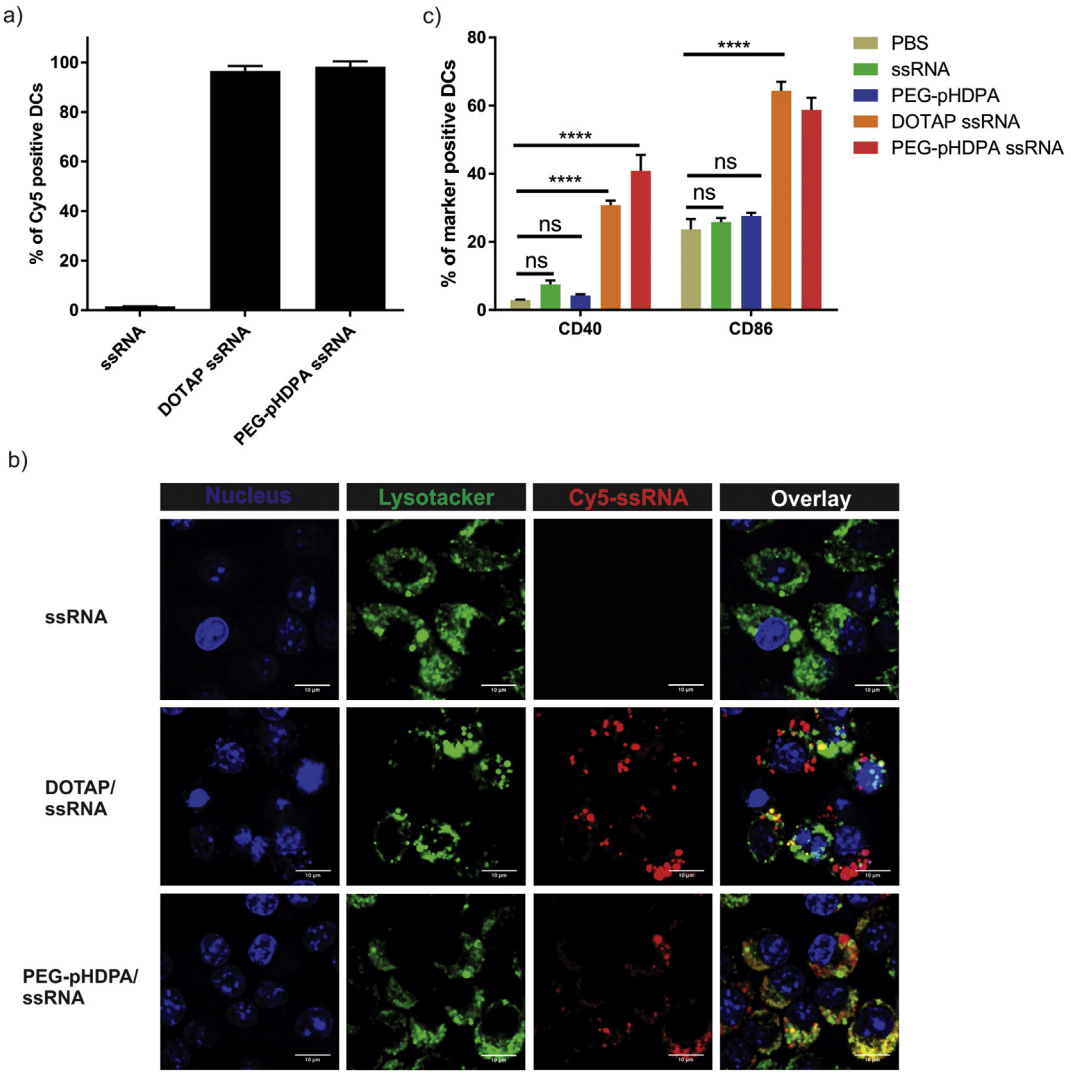

Fig. 3. Internalized ssRNA nanocomplexes promote DCs maturation in vitro. a) DC2.4 dendritic cells were incubated for 24 h with 0.25 μg Cy5-ssRNA in its free form, complexed with DOTAP, and loaded in PEG-pHDPA nanocomplexes followed by flow cytometric analysis. b) Representative confocal laser scanning images of DC2.4 cultured with indicated formulation for 24 h, bar indicated 10 μm. Yellow puncta in the overlay images indicate colocalization of ssRNA and lysotracker. c) Percentages of DC2.4 cells expressing CD40 and CD86 in response to incubation 24 h with PBS, ssRNA, PEG-pHDPA, DOTAP ssRNA and PEG-pHDPA ssRNA (herein, ssPolyU were used to form polyplexes). Two-way ANOVA analysis followed by Bonferroni multiple comparison tests (****$p < .0001$). (For interpretation of the references to color in this figure legend, the reader is referred to the web version of this article.)

failed to significantly activate DC maturation, PEG-pHDPA ssRNA nanocomplexes caused a pronounced upregulation of CD40 and CD86, which strictly is ascribed to the ssRNA loaded in the polyplexes that is released after cellular endocytosis and subsequent disulphide bonds reduction [60–63]. Importantly, PEG-pHDPA ssRNA nanocomplexes were equally potent in activation of DCs as the benchmark DOTAP ssRNA lipoplexes (Fig. 3c).

3.5. PEG-pHDPA ssRNA nanocomplexes targeting to lymph node DCs

The induction of effector T cell responses relies on the presentation of antigens by activated DCs to T cells in the draining lymph nodes. Potency of vaccines is consequently considered to benefit from strategies that augment adjuvant uptake by DCs in the draining lymph nodes, or alternatively, DCs take up the adjuvant/vaccine at the site of injection (e.g. subcutaneous injection) and then drain to the lymph nodes [64]. To investigate whether ssRNA delivery in the form of PEG-pHDPA RNA nanocomplexes would augment ssRNA uptake by lymph node DCs, we used a fluorescently labeled (Cy5) ssRNA enabling the assessment of ssRNA uptake efficiency by lymph node DCs. Cy5-ssRNA was injected either non-complexed or loaded into both PEG-pHDPA ssRNA nanocomplexes and DOTAP ssRNA lipoplexes. One day after injection, draining popliteal lymph nodes were isolated and analyzed by flow cytometry (Fig. S11). DCs were identified based on their expression of CD11c and MHCII and further subdivided into $MHCII^{int}$ DCs (blue population) and $MHCII^{hi}$ DCs (red population) (Fig. 4). Injection of ssRNA loaded in PEG-HDPA polyplexes resulted in a marked increase in numbers (and thus percentages) of lymph node DCs that contained ssRNA when compared to non-formulated ssRNA or to DOTAP ssRNA lipoplexes (Fig. 4a-c). The low accumulation of DOTAP ssRNA lipoplexes in lymph nodes can likely be ascribed to their particle size (~250 nm), since it has been shown that liposomes larger than 170 nm show poor lymphatic disposition [65]. Administration of PEG-pHDPA RNA nanocomplexes did not only result in higher numbers of Cy5-labeled ssRNA positive DCs in the draining lymph node, but also strongly increased the copies number of ssRNA endocytosed by DCs on a cell-per-cell basis as measured by the mean fluorescence intensity in the Cy5 channel (Fig. 4d). Most DCs that had internalized Cy5-ssRNA displayed a $MHCII^{hi}$ phenotype corresponding to mature DCs (Fig. 4a & b). Such $MHCII^{hi}$ DCs likely correspond to skin DCs that have migrated to the

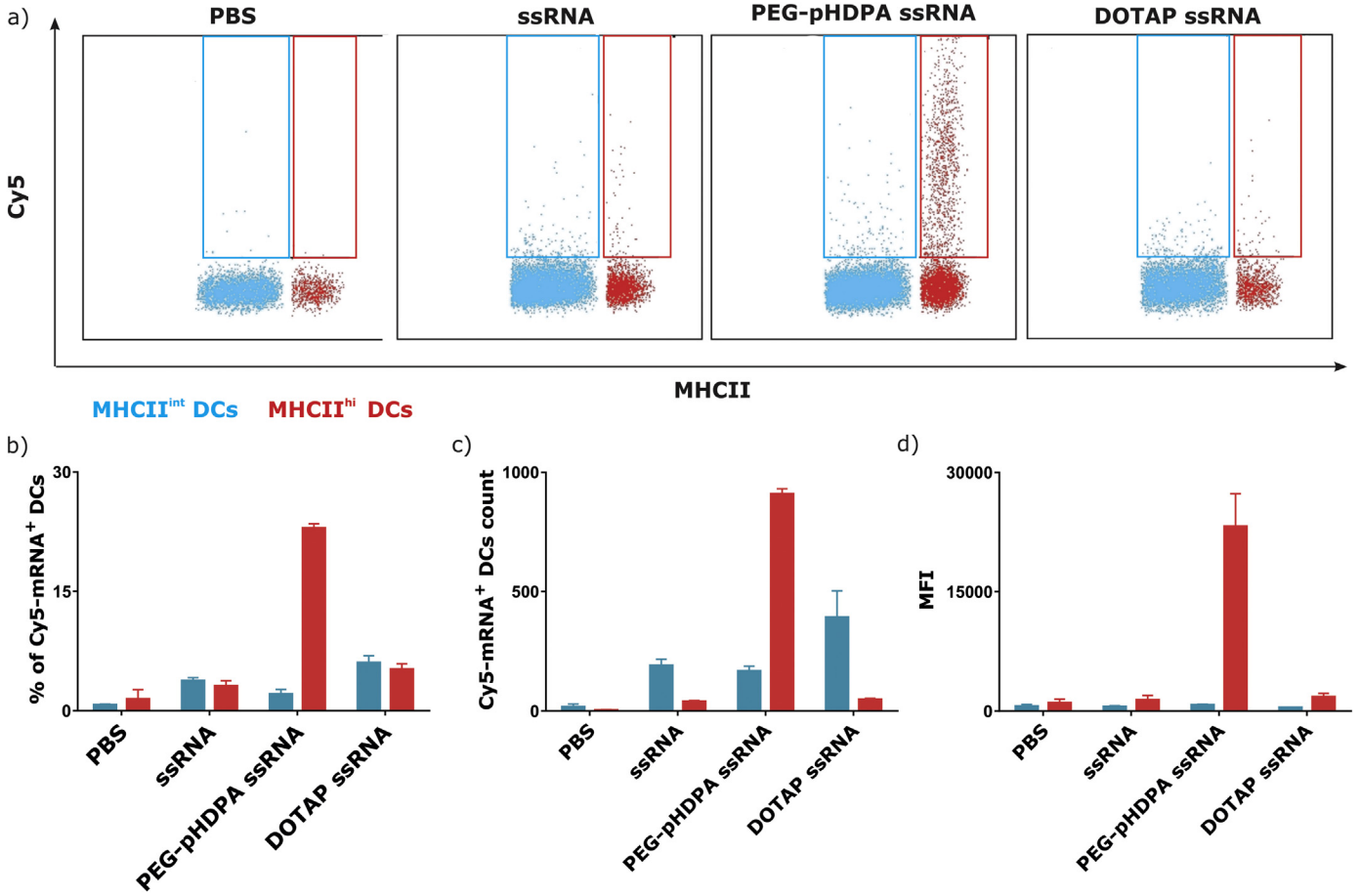

Fig. 4. ssRNA nanocomplexes efficiently target dendritic cells inside lymph nodes in vivo. Mice were s.c. injected in the footpad with PBS, 10 μg of uncomplexed ssRNA or the equivalent dose of ssRNA complexed in PEG-pHDPA ssRNA nanocomplexes or DOTAP ssRNA lipoplexes. 24 h after injection, popliteal lymph nodes were isolated and prepared for flow cytometric analysis. DCs (CD11c + MHCII+) were subdivided into $MHCII^{hi}$ DCs (red population) and into $MHCII^{int}$ DCs (blue population) and analyzed for Cy5-labeled ssRNA uptake. a) Representative flow cytometry plots. b) Percentage of Cy5-positive $MHCII^{hi}$ DCs and $MHCII^{int}$ DCs. c) Total cell count of Cy5-positive DCs. d) Mean fluorescence intensity (MFI) of the Cy5-signal of all Cy5-positive DCs. Data are presented as means ± SD of 5 mice/group. (For interpretation of the references to color in this figure legend, the reader is referred to the web version of this article.)

popliteal lymph nodes after ingestion of the PEG-pHDPA ssRNA nanocomplexes at the injection site. Alternatively, they also might represent lymph node resident DCs that have ingested the PEG-pHDPA ssRNA nanocomplexes (transported from the site of injection to these lymph nodes) and upregulated their MHCII expression. Taken together, the data of Fig. 4 shows that formulating the RNA into PEG-pHDPA ssRNA nanocomplexes substantially increases the amount of ssRNA in the target cell population - DCs - at the relevant site of T cell priming, the draining lymph node.

3.6. PEG-pHDPA ssRNA nanocomplexes promote adaptive immunity against co-delivery antigens

Inspired by the efficiently delivery of ssRNA to the draining lymph node (Fig. 4), the immune-stimulating capacity of PEG-pHDPA ssRNA nanocomplexes in vivo was assessed by *co*-injection of these polyplexes with the soluble model antigen ovalbulmin (OVA). Mice were immunized in accordance to the prime boost schedule shown in Fig. 5a. Soluble OVA was injected as saline solution or adjuvanted with respectively free ssRNA, DOTAP ssRNA lipoplexes or PEG-pHDPA ssRNA nanocomplexes. To exclude any adjuvant effects of the pHDPA and PEG, mice were immunized with OVA admixed with PEG-pHDPA without ssRNA. Six days after the booster immunization, blood was collected and the percentages OVA-specific $CD8^+$ T cells were determined via flow cytometry. As shown in Fig. 5b, solely PEG-pHDPA ssRNA nanocomplexes significantly amplified the percentages of OVA-specific $CD8^+$ T cells responses in the blood. Induction of cytolytic T cells was further assessed through an in vivo killing assay. In brief, mice were challenged two weeks after the second boost with a 1:1 ratio of OVA peptide-pulsed $CFSE^{hi}$ splenocytes (target cells) and non-pulsed $CFSE^{low}$ splenocytes (non-target cells) (Fig. 5a). Two days later, spleens were isolated and the ratio of target versus non-target cells was analyzed by flow cytometry. Mice that received OVA co-delivered with pHDPA showed no significant improvement in cytolytic T cell responses compared to mice injected with soluble OVA only (Fig. 5c), arguing against intrinsic adjuvant effects of the soluble polymer itself. When compared to mice immunized with OVA in PBS only, administration of free ssRNA did not cause a statistical significance increased cytolytic T cell response in immunized mice. Fig. 5b-e shows that injection of soluble OVA in PBS resulted in a very low immune response. Therefore, the observed antigen specific killing in some mice and Ab response in all mice are very likely due to the adjuvanticity of ssRNA. Significant increases in cytolytic responses were evoked by co-administration of OVA with DOTAP ssRNA lipoplexes, but importantly, the most robust cytolytic T cell responses were clearly achieved when using PEG-pHDPA ssRNA nanocomplexes as adjuvant. The humoral immune responses using ssRNA as an adjuvant was also investigated. Mice immunized with ssRNA as adjuvant - regardless of the format the ssRNA was delivered into - showed a strong increase in IgG1 titers (Fig. 5d). Loading of ssRNA into PEG-pHDPA nanocomplexes strongly promoted

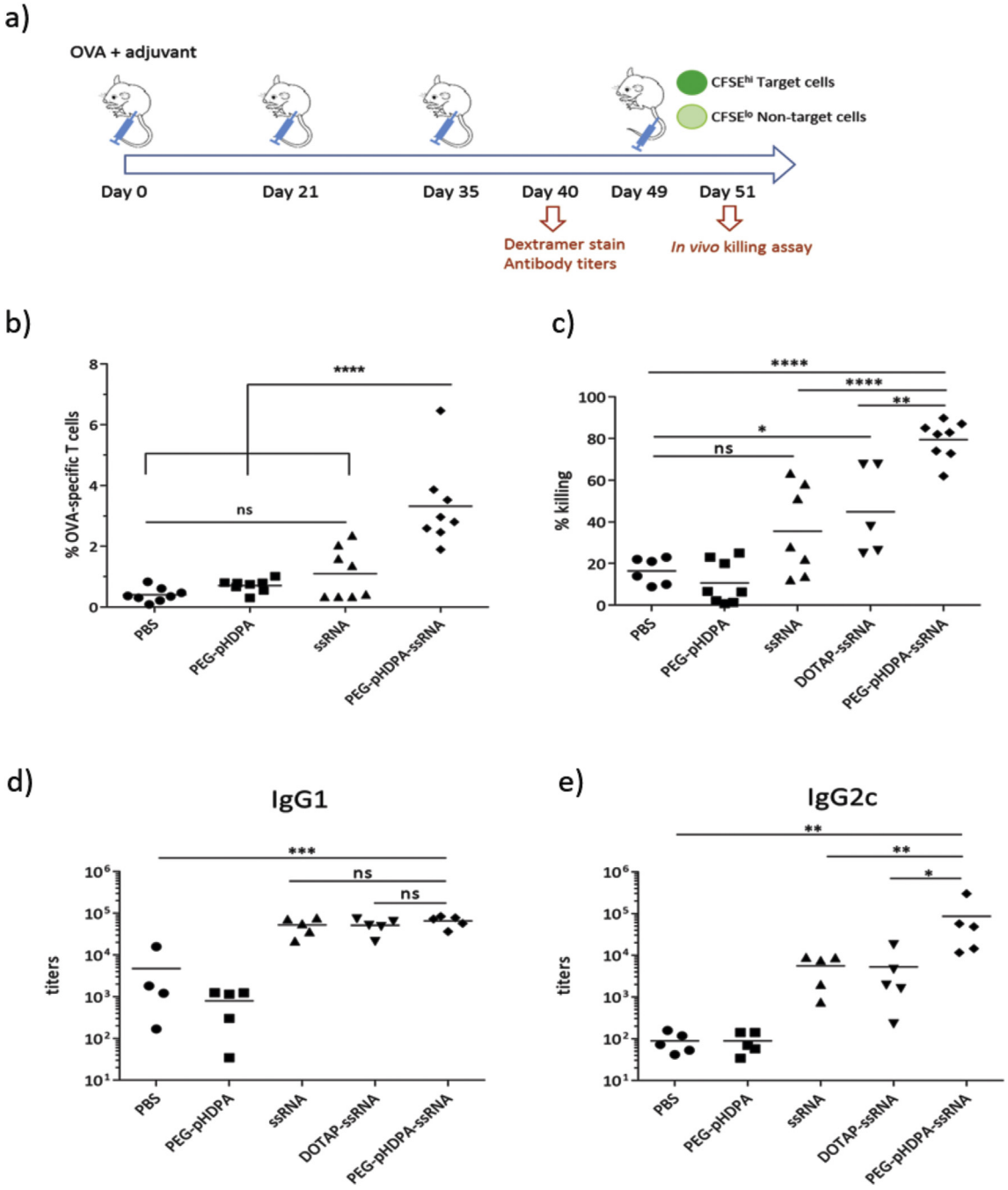

Fig. 5. Adaptive immune responses evoked by PEG-pHDPA ssRNA nanocomplexes adjuvanted protein vaccination. a) Immunization schedule and experimental set up. b) Percentages of OVA-specific CD8+ T cells induced by immunization with the indicated OVA/adjuvant formulations. Data are shown as means of 8 mice per group. c) Specific killing of target cells in response to each vaccine formulation. % killing was calculated using the formula: 100–100 × ((CFSEhigh/CFSElow) immunized mice / (CFSEhigh/CFSElow) non-immunized mice). Data are shown as means of 6–8 mice/group. Antibody titers of IgG1 (d) and IgG2c (e) as measured by ELISA in response to the indicated OVA/adjuvant formulations. Data are shown as means of 4–5 mice per group. *$p < .05$; **$p < .01$; ***$p < .001$; ****$p < .0001$ (one-way ANOVA).

antibody isotype switching to IgG2c - a feature dependent of IFN-γ and indicative for the induction of Th1 immunity [66]. As can be appreciated from Fig. 5e, PEG-pHDPA ssRNA nanocomplexes were more potent at instigating IgG2c compared to free or DOTAP complexed ssRNA.

4. Conclusions

In summary, we have developed and demonstrated an alternative way to post-functionalize polyplexes via copper-free click chemistry. After post-PEGylation, the near neutral polyplexes were colloidal stable and able to protect the RNA against enzymatic degradation. PEG-pHDPA ssRNA nanocomplexes were efficiently taken up by DCs and promote DC maturation in vitro. More importantly, up to 25–30% of DCs in the lymph nodes had internalized the ssRNA nanocomplexes, and thereafter were able to efficiently promote adaptive immunity against co-delivered antigens, which points that PEG-pHDPA ssRNA nannocomplexes are an attractive candidate as novel adjuvant.

Conflict of interest

The authors declare no competing financial interest.

Acknowledgment

Bo Lou was funded by China Scholarship Council. This work was supported by grants from the UGhent Concerted Research Consortium BOF12/GOA-B/12424/01, the Fund for Scientific Research Flanders project G.0226.10. De Beuckelaer A. acknowledges IWT (Agentschap voor innovatie door wetenschap en technologie, Vlaanderen) for a PhD scholarship.

Appendix A. Supplementary data

Supplementary data to this article can be found online at https://doi.org/10.1016/j.jconrel.2018.06.010.

References

[1] R.L. Coffman, A. Sher, R.A. Seder, Vaccine adjuvants: putting innate immunity to work, Immunity 33 (2010) 492–503.
[2] W.C. Koff, D.R. Burton, P.R. Johnson, B.D. Walker, C.R. King, G.J. Nabel, R. Ahmed, M.K. Bhan, S.A. Plotkin, Accelerating next-generation vaccine development for global disease prevention, Science 340 (2013) 1232910-1–1232910-7.
[3] R. Arens, T. van Hall, S.H. van der Burg, F. Ossendorp, C.J.M. Melief, Prospects of combinatorial synthetic peptide vaccine-based immunotherapy against cancer, Semin. Immunol. 25 (2013) 182–190.
[4] R.J. Mancini, L. Stutts, K.A. Ryu, J.K. Tom, A.P. Esser-Kahn, Directing the immune system with chemical compounds, ACS Chem. Biol. 9 (2014) 1075–1085.
[5] K. Kastenmüller, U. Wille-Reece, R.W.B. Lindsay, L.R. Trager, P.A. Darrah, B.J. Flynn, M.R. Becker, M.C. Udey, B.E. Clausen, B.Z. Igyarto, D.H. Kaplan, W. Kastenmüller, R.N. Germain, R.A. Seder, Protective T cell immunity in mice following protein-TLR7/8 agonist-conjugate immunization requires aggregation, type I IFN, and multiple DC subsets, J. Clin. Invest. 121 (2011) 1782–1796.
[6] R. Heidenreich, E. Jasny, A. Kowalczyk, J. Lutz, J. Probst, P. Baumhof, B. Scheel, S. Voss, K.J. Kallen, M. Fotin-Mleczek, A novel RNA-based adjuvant combines strong immunostimulatory capacities with a favorable safety profile, Int. J. Cancer 137 (2015) 372–384.
[7] A. Kowalczyk, F. Doener, K. Zanzinger, J. Noth, P. Baumhof, M. Fotin-Mleczek, R. Heidenreich, Self-adjuvanted mRNA vaccines induce local innate immune responses that lead to a potent and boostable adaptive immunity, Vaccine 34 (2016) 3882–3893.
[8] S.S. Diebold, T. Kaisho, H. Hemmi, S. Akira, C. Reis E. Sousa, Innate antiviral responses by means of TLR7-mediated recognition of single-stranded RNA, Science 303 (2004) 1529–1531.
[9] L.M. Kranz, M. Diken, H. Haas, S. Kreiter, C. Loquai, K.C. Reuter, M. Meng, D. Fritz, F. Vascotto, H. Hefesha, C. Grunwitz, M. Vormehr, Y. Hüsemann, A. Selmi, A.N. Kuhn, J. Buck, E. Derhovanessian, R. Rae, S. Attig, J. Diekmann, R.A. Jabulowsky, S. Heesch, J. Hassel, P. Langguth, S. Grabbe, C. Huber, Ö. Türeci, U. Sahin, Systemic RNA delivery to dendritic cells exploits antiviral defence for cancer immunotherapy, Nature 534 (2016) 396–401.
[10] D. Rajagopal, C. Paturel, Y. Morel, S. Uematsu, S. Akira, S.S. Diebold, Plasmacytoid dendritic cell-derived type I interferon is crucial for the adjuvant activity of toll-like receptor 7 agonists, Blood 115 (2010) 1949–1957.
[11] A.E. Sköld, J.J.P. van Beek, S.P. Sittig, G. Bakdash, J. Tel, G. Schreibelt, I.J.M. de Vries, Protamine-stabilized RNA as an ex vivo stimulant of primary human dendritic cell subsets, Cancer Immunol. Immunother. 64 (2015) 1461–1473.
[12] J.H. van den Berg, K. Oosterhuis, W.E. Hennink, G. Storm, L.J. van der Aa, J.F.J. Engbersen, J.B.A.G. Haanen, J.H. Beijnen, T.N. Schumacher, B. Nuijen, Shielding the cationic charge of nanoparticle-formulated dermal DNA vaccines is essential for antigen expression and immunogenicity, J. Control. Release 141 (2010) 234–240.
[13] R.N. Palumbo, X. Zhong, D. Panus, W. Han, W. Ji, C. Wang, Transgene expression and local tissue distribution of naked and polymer-condensed plasmid DNA after intradermal administration in mice, J. Control. Release 159 (2012) 232–239.
[14] R. Tang, R.N. Palumbo, L. Nagarajan, E. Krogstad, C. Wang, Well-defined block copolymers for gene delivery to dendritic cells: probing the effect of polycation chain-length, J. Control. Release 142 (2010) 229–237.
[15] J.S. Suk, Q. Xu, N. Kim, J. Hanes, L.M. Ensign, PEGylation as a strategy for improving nanoparticle-based drug and gene delivery, Adv. Drug Deliv. Rev. 99 (2016) 28–51.
[16] S. De Koker, J. Cui, N. Vanparijs, L. Albertazzi, J. Grooten, F. Caruso, B.G. De Geest, Engineering polymer hydrogel nanoparticles for lymph node-targeted delivery, Angew. Chem. Int. Ed. 55 (2016) 1334–1339.
[17] H. Jiang, Q. Wang, L. Li, Q. Zeng, H. Li, T. Gong, Z. Zhang, X. Sun, Turning the old adjuvant from gel to nanoparticles to amplify CD8 + T cell responses, Adv. Sci. 5 (2017) 1700426.
[18] C.H. Ahn, S.Y. Chae, Y.H. Bae, S.W. Kim, Synthesis of biodegradable multi-block copolymers of poly(L-lysine) and poly(ethylene glycol) as a non-viral gene carrier, J. Control. Release 97 (2004) 567–574.
[19] R.J. Christie, Y. Matsumoto, K. Miyata, T. Nomoto, S. Fukushima, K. Osada, J. Halnaut, F. Pittella, H.J. Kim, N. Nishiyama, K. Kataoka, Targeted polymeric micelles for siRNA treatment of experimental cancer by intravenous injection, ACS Nano 6 (2012) 5174–5189.
[20] S. Uchida, H. Kinoh, T. Ishii, A. Matsui, T.A. Tockary, K.M. Takeda, H. Uchida, K. Osada, K. Itaka, K. Kataoka, Systemic delivery of messenger RNA for the treatment of pancreatic cancer using polyplex nanomicelles with a cholesterol moiety, Biomaterials 82 (2016) 221–228.
[21] Z. Ge, Q. Chen, K. Osada, X. Liu, T.A. Tockary, S. Uchida, A. Dirisala, T. Ishii, T. Nomoto, K. Toh, Y. Matsumoto, M. Oba, M.R. Kano, K. Itaka, K. Kataoka, Targeted gene delivery by polyplex micelles with crowded PEG palisade and cRGD moiety for systemic treatment of pancreatic tumors, Biomaterials 35 (2014) 3416–3426.
[22] C. Lin, J.F.J. Engbersen, PEGylated bioreducible poly(amido amine)s for non-viral gene delivery, Mater. Sci. Eng. C 31 (2011) 1330–1337.
[23] P. Vader, L.J. Van Der Aa, J.F.J. Engbersen, G. Storm, R.M. Schiffelers, Physicochemical and biological evaluation of siRNA polyplexes based on PEGylated poly(amido amine)s, Pharm. Res. 29 (2012) 352–361.
[24] H.-K. Nguyen, P. Lemieux, S.V. Vinogradov, C.L. Gebhart, N. Guerin, G. Paradis, T.K. Bronich, V.Y. Alakhov, A.V. Kabanov, Evaluation of polyether-poly-ethylenimine graft copolymers as gene transfer agents, Gene Ther. 7 (2000) 126–138.
[25] C. Zhang, S. Gao, W. Jiang, S. Lin, F. Du, Z. Li, W. Huang, Targeted minicircle DNA delivery using folate-poly(ethylene glycol)-polyethylenimine as non-viral carrier, Biomaterials 31 (2010) 6075–6086.
[26] P. Erbacher, T. Bettinger, P. Belguise-Valladier, S. Zou, J.L. Coll, J.P. Behr, J.S. Remy, Transfection and physical properties of various saccharide, poly(ethylene glycol), and antibody-derivatized polyethylenimines (PEI), J. Gene Med. 1 (1999) 210–222.
[27] K.M. Takeda, K. Osada, T.A. Tockary, A. Dirisala, Q. Chen, K. Kataoka, Poly(ethylene glycol) crowding as critical factor to determine pDNA packaging scheme into polyplex micelles for enhanced gene expression, Biomacromolecules 18 (2017) 36–43.
[28] J.-M. Williford, Y. Ren, K. Huang, D. Pan, H.-Q. Mao, Shape transformation following reduction-sensitive PEG cleavage of polymer/DNA nanoparticles, J. Mater. Chem. B 2 (2014) 8106–8109.
[29] T. Blessing, M. Kursa, R. Holzhauser, R. Kircheis, E. Wagner, Different strategies for formation of PEGylated EGF-conjugated PEI/DNA complexes for targeted gene delivery, Bioconjug. Chem. 12 (2001) 529–537.
[30] F.J. Verbaan, C. Oussoren, C.J. Snel, D.J.A. Crommelin, W.E. Hennink, G. Storm, Steric stabilization of poly(2-(dimethylamino)ethyl methacrylate)-based polyplexes mediates prolonged circulation and tumor targeting in mice, J. Gene Med. 6 (2004) 64–75.
[31] Y. Jiang, J. Chen, C. Deng, E.J. Suuronen, Z. Zhong, Click hydrogels, microgels and nanogels: emerging platforms for drug delivery and tissue engineering, Biomaterials 35 (2014) 4969–4985.
[32] J. Dommerholt, O. Van Rooijen, A. Borrmann, C.F. Guerra, F.M. Bickelhaupt, F.L. Van Delft, Highly accelerated inverse electron-demand cycloaddition of electron-deficient azides with aliphatic cyclooctynes, Nat. Commun. 5 (2014) 1–7.
[33] J. Dommerholt, S. Schmidt, R. Temming, L.J.A. Hendriks, F.P.J.T. Rutjes, J.C.M. Van Hest, D.J. Lefeber, P. Friedl, F.L. Van Delft, Readily accessible bicyclononynes for bioorthogonal labeling and three-dimensional imaging of living cells, Angew. Chem. Int. Ed. 49 (2010) 9422–9425.
[34] L. Novo, L.Y. Rizzo, S.K. Golombek, G.R. Dakwar, B. Lou, K. Remaut, E. Mastrobattista, C.F. Van Nostrum, W. Jahnen-Dechent, F. Kiessling, K. Braeckmans, T. Lammers, W.E. Hennink, Decationized polyplexes as stable and safe carrier systems for improved biodistribution in systemic gene therapy, J. Control. Release 195 (2014) 162–175.
[35] L. Novo, E.V.B. van Gaal, E. Mastrobattista, C.F. van Nostrum, W.E. Hennink, Decationized crosslinked polyplexes for redox-triggered gene delivery, J. Control. Release 169 (2013) 246–256.
[36] L. Novo, K.M. Takeda, T. Petteta, G.R. Dakwar, J.B. Van Den Dikkenberg, K. Remaut, K. Braeckmans, C.F. Van Nostrum, E. Mastrobattista, W.E. Hennink, Targeted decationized polyplexes for siRNA delivery, Mol. Pharm. 12 (2015) 150–161.
[37] A.M. Funhoff, C.F. van Nostrum, M.C. Lok, J.A.W. Kruijtzer, D.J.A. Crommelin, W.E. Hennink, Cationic polymethacrylates with covalently linked membrane destabilizing peptides as gene delivery vectors, J. Control. Release 101 (2005) 233–246.
[38] A.M. Funhoff, C.F. Van Nostrum, A.P.C.A. Janssen, M.H.A.M. Fens, D.J.A. Crommelin, W.E. Hennink, Polymer side-chain degradation as a tool to control the destabilization of polyplexes, Pharm. Res. 21 (2004) 170–176.
[39] J. Kopecek, P. Kopecková, HPMA copolymers: origins, early developments, present, and future, Adv. Drug Deliv. Rev. 62 (2010) 122–149.
[40] B. Říhová, M. Kovář, Immunogenicity and immunomodulatory properties of HPMA-based polymers, Adv. Drug Deliv. Rev. 62 (2010) 184–191.
[41] G.T. Zugates, D.G. Anderson, S.R. Little, I.E.B. Lawhorn, R. Langer, Synthesis of poly (beta-amino ester)s with thiol-reactive side chains for DNA delivery, J. Am. Chem. Soc. 128 (2006) 12726–12734.
[42] M.F. Ebbesen, D.H. Schaffert, M.L. Crowley, D. Oupický, K.A. Howard, Synthesis of click-reactive HPMA copolymers using RAFT polymerization for drug delivery applications, J. Polym. Sci. Part A Polym. Chem. 51 (2013) 5091–5099.
[43] X. Jiang, A. van der Horst, M.J. van Steenbergen, N. Akeroyd, C.F. van Nostrum, P.J. Schoenmakers, W.E. Hennink, Molar-mass characterization of cationic polymers for gene delivery by aqueous size-exclusion chromatography, Pharm. Res. 23

(2006) 595–603.
[44] Y. Yue, F. Jin, R. Deng, J. Cai, Y. Chen, M.C.M. Lin, H.F. Kung, C. Wu, Revisit complexation between DNA and polyethylenimine - effect of uncomplexed chains free in the solution mixture on gene transfection, J. Control. Release 155 (2011) 67–76.
[45] G.R. Dakwar, K. Braeckmans, J. Demeester, W. Ceelen, S.C. De Smedt, K. Remaut, Disregarded effect of biological fluids in siRNA delivery: human ascites fluid severely restricts cellular uptake of nanoparticles, ACS Appl. Mater. Interfaces 7 (2015) 24322–24329.
[46] H. Takemoto, K. Miyata, T. Ishii, S. Hattori, S. Osawa, N. Nishiyama, K. Kataoka, Accelerated polymer − polymer click conjugation by freeze − thaw treatment, Bioconjug. Chem. 23 (2012) 1503–1506.
[47] R.J. Christie, K. Miyata, Y. Matsumoto, T. Nomoto, D. Menasco, T.C. Lai, M. Pennisi, K. Osada, S. Fukushima, N. Nishiyama, Y. Yamasaki, K. Kataoka, Effect of polymer structure on micelles formed between siRNA and cationic block copolymer comprising thiols and amidines, Biomacromolecules 12 (2011) 3174–3185.
[48] M. Neu, O. Germershaus, M. Behe, T. Kissel, Bioreversibly crosslinked polyplexes of PEI and high molecular weight PEG show extended circulation times in vivo, J. Control. Release 124 (2007) 69–80.
[49] J.-H. Ryu, R.T. Chacko, S. Jiwpanich, S. Bickerton, R.P. Babu, S. Thayumanavan, Self-cross-linked polymer nanogels: a versatile nanoscopic drug delivery platform, J. Am. Chem. Soc. 132 (2010) 17227–17235.
[50] Y. Niebel, M.D. Buschmann, M. Lavertu, G. De Crescenzo, Combined analysis of polycation/ODN polyplexes by analytical ultracentrifugation and dynamic light scattering reveals their size, refractive index increment, stoichiometry, porosity, and molecular weight, Biomacromolecules 15 (2014) 940–947.
[51] S.M. Zou, P. Erbacher, J.S. Remy, J.P. Behr, Systemic linear polyethylenimine (L-PEI)-mediated gene delivery in the mouse, J. Gene Med. 2 (2000) 128–134.
[52] S. Boeckle, K. von Gersdorff, S. van der Piepen, C. Culmsee, E. Wagner, M. Ogris, Purification of polyethylenimine polyplexes highlights the role of free polycations in gene transfer, J. Gene Med. 6 (2004) 1102–1111.
[53] K. Braeckmans, K. Buyens, B. Naeye, D. Vercauteren, H. Deschout, K. Raemdonck, K. Remaut, N.N. Sanders, J. Demeester, S.C. De Smedt, Advanced fluorescence microscopy methods illuminate the transfection pathway of nucleic acid nanoparticles, J. Control. Release 148 (2010) 69–74.
[54] K. Braeckmans, K. Buyens, W. Bouquet, C. Vervaet, P. Joye, F. De Vos, L. Plawinski, L. Doeuvre, E. Angles-Cano, N.N. Sanders, J. Demeester, S.C. De Smedt, Sizing nanomatter in biological fluids by fluorescence single particle tracking, Nano Lett. 10 (2010) 4435–4442.
[55] V. Filipe, A. Hawe, W. Jiskoot, Critical evaluation of nanoparticle tracking analysis (NTA) by NanoSight for the measurement of nanoparticles and protein aggregates, Pharm. Res. 27 (2010) 796–810.
[56] M. Sioud, Innate sensing of self and non-self RNAs by toll-like receptors, Trends Mol. Med. 12 (2006) 167–176.
[57] M.O. Oyewumi, A. Kumar, Z. Cui, Nano-microparticles as immune adjuvants: correlating particle sizes and the resultant immune responses, Expert Rev. Vaccines 9 (2010) 1095–1107.
[58] J. Luten, N. Akeroyd, A. Funhoff, M.C. Lok, H. Talsma, W.E. Hennink, Methacrylamide polymers with hydrolysis-sensitive cationic side groups as degradable gene carriers, Bioconjug. Chem. 17 (2006) 1077–1084.
[59] M.C. Kerr, M.R. Lindsay, R. Luetterforst, N. Hamilton, F. Simpson, R.G. Parton, P.A. Gleeson, R.D. Teasdale, Visualisation of macropinosome maturation by the recruitment of sorting nexins, J. Cell Sci. 119 (2006) 3967–3980.
[60] J. Yang, H. Chen, I.R. Vlahov, J.-X. Cheng, P.S. Low, Evaluation of disulfide reduction during receptor-mediated endocytosis by using FRET imaging, Proc. Natl. Acad. Sci. 103 (2006) 13872–13877.
[61] F. Meng, W.E. Hennink, Z. Zhong, Reduction-sensitive polymers and bioconjugates for biomedical applications, Biomaterials 30 (2009) 2180–2198.
[62] L. Brülisauer, M.A. Gauthier, J.C. Leroux, Disulfide-containing parenteral delivery systems and their redox-biological fate, J. Control. Release 195 (2014) 147–154.
[63] Y. Song, B. Lou, P. Zhao, C. Lin, Multifunctional disulfide-based cationic dextran conjugates for intravenous gene delivery targeting ovarian cancer cells, Mol. Pharm. 11 (2014) 2250–2261.
[64] S. Rahimian, J.W. Kleinovink, M.F. Fransen, L. Mezzanotte, H. Gold, P. Wisse, H. Overkleeft, M. Amidi, W. Jiskoot, C.W. Löwik, F. Ossendorp, W.E. Hennink, Near-infrared labeled, ovalbumin loaded polymeric nanoparticles based on a hydrophilic polyester as model vaccine: in vivo tracking and evaluation of antigen-specific CD8+ T cell immune response, Biomaterials 37 (2015) 469–477.
[65] C. Oussoren, J. Zuidema, D.J.A. Crommelin, G. Storm, Lymphatic uptake and biodistribution of liposomes after subcutaneous injection. II. Influence of liposomal size, lipid composition and lipid dose, Biochim. Biophys. Acta 1328 (1997) 261–272.
[66] N.P.H. Knudsen, A. Olsen, C. Buonsanti, F. Follmann, Y. Zhang, R.N. Coler, C.B. Fox, A. Meinke, U. D'Oro, D. Casini, A. Bonci, R. Billeskov, E. De Gregorio, R. Rappuoli, A.M. Harandi, P. Andersen, E.M. Agger, Different human vaccine adjuvants promote distinct antigen-independent immunological signatures tailored to different pathogens, Sci. Rep. 6 (2016) 19570.